The electric field at the apex of a near-field probe: implications for nanoRaman spectroscopy

H.D. Hallen, North Carolina State University, Raleigh, NC 27695
C.L. Jahncke, St. Lawrence University, Canton, NY 13617

Abstract

Near-field or nano-Raman spectroscopy is different from its far-field counterpart in several important respects. We present a unified view of nano-Raman that accounts for these differences, which include surface enhancement, propagation differences, the presence of z-polarized light, as well as electric field gradients that give rise to new spectroscopic selection rules. We also discuss some of the recent advances in near-field scanning optical microscopy (NSOM) and their positive impact on nano-Raman spectroscopy. In particular progress has been made in fabricating better probes, both apertured and apertureless, for NSOM resulting in larger signal levels important for Raman spectroscopy. Larger signals result in shorter imaging times, the ability to achieve higher resolution, and broader applicability of the technique.

Keywords: NSOM, SNOM, Raman Near-field

Hans Hallen
Box 8202 Physics Department
North Carolina State University
Raleigh, NC 27695
Phone: (919) 515-6314
Fax: (919) 515-7331
Email: Hans_Hallen@ncsu.edu

Introduction.

Within the past 7-10 years, we have witnessed the birth of nano-Raman spectroscopy. It represents one of the few techniques that yields chemical information at nanoscale length scales without damaging the sample. It began with performing Raman using the near-field scanning optical microscopes (NSOMs) available at the time [1], and has benefited from advances to NSOM during the intervening years. This has resulted in the exploitation of new probe designs [2]and utilizing the inverse of an aperture, a pointed conducting tip--an apertureless NSOM[3]. Studies [4-7] have shown that nano-Raman spectra are different from far-field Raman due to the inherent requirement of a conductor in proximity to the surface to localize the electromagnetic interaction. This differs from the advance to micro Raman from macro Raman that showed essentially the same spectroscopy. We discuss in this paper the various features or properties of nano-Raman spectroscopy and imaging that have become evident in the last several years to give a comprehensive picture of what a nano-Raman practitioner needs to consider.

Nano-Raman spectroscopy retains most of the advantages of its far-field counterparts while improving resolution and providing a topographic image to corroborate the optical data. Raman spectroscopy is a powerful technique for characterizing materials. It enables the determination of sample composition, chemical bonding, material structure, phase, and induced stress. In fact, near-field Raman has been used to study localized stress [8], local chemical composition [9, 10], and local material composition [11] to name a few applications. Nano-Raman, as far-field Raman, is advantageous in that it can be performed under ambient conditions. No special sample preparation is required. Further, the visible light is not as damaging to a sample as are more energetic photons or electrons. Resolution was the initial goal of nano-Raman, expected since NSOM can provide optical information with a resolution of $\lambda/20$[12, 13]; this is an order of magnitude larger than the best conventional optical microscopy. However, the reason that the combination of these two techniques has not been applied more broadly lies in the fact that the signals are very small. Raman spectroscopy has a very small scattering cross-section; typically one in a million photons is Raman scattered. NSOM also suffers from low signal levels; typically only 10's of nanowatts are at the fiber aperture. The combination of these two techniques, therefore, results in very low signal levels. We will comment throughout the paper on recent advances that have helped to make near-field Raman more accessible.

Near-field scanning optical microscopy.

Near-field scanning optical microscopy is one in a family of scanned probe techniques that includes scanning tunneling microscopy and atomic force microscopy (AFM) where an image is obtained by raster scanning a probe across a surface collecting data at an array of points during the scan. The scanned probe in NSOM experiments is typically a sharpened optical fiber that has been coated with a metal, such as aluminum, to create an aperture. The fiber can be used as a light source (illumination mode) or detector (collection mode), and experiments can be performed in transmission or reflection, see figure 1[14, 15]. The resolution is limited by the size of the aperture up to a certain point, 10 to 20 nm, after which the electric field spreads out and resolution is lost. The probe must be in close proximity to the sample surface because the electric

field spreads out rapidly as a function of distance from the aperture. Spectroscopic studies can be done by directing the collected light, either from the probe in the near-field (collection mode) or a detector in the far field (illumination mode), into a spectrometer.

An alternate way to do near-field microscopy, termed apertureless NSOM, is to place a sharpened metal probe close to a sample in a region illuminated by the optical field [3, 16]. In this case there is a field enhancement due to the sharp probe. Several geometries have been used with apertureless NSOM. The sample may be illuminated from below via total internal reflection or a high N.A. objective while the probe is incident from above, see figure 1. Or the sample may be illuminated obliquely from above with the tip also above the surface. Positioning the tip offset laterally from the center of a focussed coaxial beam also works[17]. In all cases, a component of the electric field must exist along the axis of the probe to excite the surface plasmons thought to be primarily responsible for the enhancement of the signal. Therefore, the incident light is p-polarized. This results in the presence of two components of the electric field at the sample surface, one in the plane of the surface and one perpendicular to it. Calculations of the local field enhancement under the apertureless probe predict a factor of 44 improvement over the signal without the probe[18].

Raman imaging advances

Early work in near-field Raman spectroscopy/microscopy was hindered by very low signal levels. Collecting the data for the first near-field image in a Raman line took over 10 hours [1]. Additionally, the low signal levels made achieving the high resolutions available with NSOM very difficult; large aperture probes were needed to obtain enough signal. Recent advances in near-field Raman imaging primarily involve improving the near-field signal and/or the Raman signal (other advances -- understanding the spectra, are discussed in other sections). Higher signals result in shorter data collection times and higher resolution. Studying strong Raman scatterers obviously improves the Raman signal. Resonance Raman and surface enhanced Raman scattering (SERS) also give larger Raman signals. We will look at the improvement of the near-field signal and Raman signal as it has been attacked on two fronts. The first involves fabricating better fiber optic probes with higher throughput than the probes formed by heating and pulling. The second involves using apertureless probes.

Early near-field Raman used probes made from optical fibers with tips formed by heating and pulling the glass[19]; apertures were formed by subsequently coating the probes with aluminum. The probes made with the heating and pulling process are characterized by long tapers and small cone angles. Due to the evanescent nature of the optical signal traveling down the tapered region, much of the light is lost[20]. Probe fabrications has been dramatically improved with chemical etching [21] which produces fibers with shorter tapers and larger cone angles. However, the surface of the cone can be of poor quality unless the utmost care is taken in vibration, wind, and acoustic isolation of the apparatus (usually in a hood!). Suh and Zenobi have developed a method where the advantages of etching are retained and the reproducibility of the cone surface quality is improved [22]. Essentially, they etch the fiber without removing the plastic fiber jacket, and they are able to obtain a damage threshold of a laser intensity of 10^8 W/cm^2 at

the aperture. Another interesting method that utilizes the same qualitative idea as the etched fibers (minimize the region in which light reflects from metal to that in which total internal reflection will not work) is to coat only the last 10 or so microns of the tip with metal[2]. These ring tips show improved optical throughput, but to our knowledge have not been used with nano-Raman spectroscopy.

The chemically etched probes have been improved upon in additional ways. The essential idea is to make a probe that acts like a surface enhanced Raman scattering surface. Instead of depositing the desired sample onto a surface of silver or gold colloids, the probe acts as the source of colloids where the light would be amplified by the surface plasmon resonance of the metal nanostructures. Sqalli et al. have attached a single gold particle at the apex of the aluminum coated etched optical fibers and see a factor of 2 to 10 increase in signal along with a depolarization of the light as seen in the far field [23]. This depolarization is consistent with predictions based on Mie theory. Michaels et al. coated the fiber probe with a layer of discrete silver islands in order to create a SERS probe [24]. The idea is that one of the silver colloids will form near the fiber apex providing a local field enhancement near the surface being studied. They used these probes to study the Raman signal on single crystal diamond, and they noted an enhancement of a factor of 6 over the same probe without the metal colloids. The signal was somewhat unstable and the enhancement was smaller than expected, however, it still represents an improvement in signal.

As we have seen, the primary difficulty with the metal-coated fibers is getting enough light through them. To circumvent this problem, one can do apertureless NSOM. In this case an opaque sharpened probe is used in place of the optical fiber. The sharpened probe may be made of metal, dielectric or semiconductor. Because of the enhancement due to surface plasmons (and the potential for SERS, in Raman applications), the sharp probe is typically made of metal or coated with metal [25-27]. Stöckle et al. report a factor of 30 increase in the Raman signal when the metalized AFM tip (50nm diameter) was brought close to the laser illuminated (300nm diameter) sample, a thin film of brilliant cresyl blue. The overall enhancement is larger than just the signal increase because the area being illuminated by the light source is much larger than the area under the probe. When the tip diameter and the laser spot size are taken into account they found the enhancement to be a factor of 2000. They also used a sharpened gold wire (20nm diameter) to measure the Raman signal on C^{60}. The signal increased by approximately a factor of 40. (This was difficult to determine due to the lack of Raman signal without the presence of the fiber.) When the laser spot size and tip diameter were taken into account, an enhancement of over 40,000 was obtained. The Raman signal in this case was determined to come from a spot size of 55 nm in diameter. Both Anderson and Stöckle observe cases where there is almost no Raman signal until the probe is brought into the near-field of the sample making enhancement factors difficult to calculate. These improvements in signal are accompanied by shorter sampling times and higher resolution.

Raman imaging has recently undergone steady progress with regard to improved resolution and imaging time, however, there remain very few Raman images in the

literature. We obtained the first near-field image in Raman line in 1995[1]. In 1997 near-field Raman with fiber probes was combined with surface enhancement techniques to generate large signals and shorter integration times[28]. In 1998 Deckert et al. pushed the SERS nano-Raman even further and obtained 100 nm resolution on Dye Labeled DNA [29]. More recently Gucciardi et al. published Raman images on TCNQ thin films where they were able to easily distinguish the Cu-TCNQ clusters from the film [9]. With regard to Raman imaging using apertureless probes, Hayazawa et al. use a silver coated AFM cantilever to do SERS imaging on samples with molecules of both Rhodamine6G and Crystal Violet. The images were 1 μm square and the acquisition time was 10 minutes[30]. This is a significant improvement over the earlier images.

Electric Field near the Probe

Boundary Conditions

Maxwell's equations determine the boundary condition near a metal surface, such as the metal making the probe aperture or the tip of the apertureless probe. The electric field must be normal to the surface. Currents flow to eliminate electric field tangent to the surface. For real conductors, finite charge density results in a penetration depth of a few nanometers for the electric field in to the metal. This already gives a reasonable qualitative picture of the fields emanating from an apertured probe: the electric field under immediately under the aperture is polarized as the light input to the aperture is (although it is not the same as that input to the fiber due to the large angle reflections from metal in the structure that tend to convert linearly polarized light into nearly circular elliptically polarized light**).** The light 'ray' must bend beneath the probe, however, to produce axial or z-polarized light under the metal so that the boundary condition is satisfied. We see this behavior in the calculated fields, which follow.

Model Calculation

There are many papers that calculate the electric fields beneath an apertured or apertureless NSOM probe, for example, see[31, 32]. We will not present another theory, but rather show the results of the simpler Bethe-Bouwkamp model for the electric fields near a small hole in a perfectly conducting plane[33, 34]. This model was used by Betzig et al. to compare with measurements of single molecule fluorescence, with which good agreement was found. Figure 2 shows calculations of the profile of various components of the electric field squared [6] in a plane a distance 10 nm (left) or 1 nm (right) below the aperture. The aperture used was 200 nm and the wavelength 514 nm. The probe is along the z-axis, and the light shining on the aperture is polarized in the x direction. The region shown is twice the aperture size square. We see that the predictions are valid. Near the aperture, we see that indeed all polarization components of the light are present. As expected, the z-polarized light exists under the metal forming the aperture, and x-y polarized light exists under the aperture itself. Far from the aperture, if no sample is in place, the light from the aperture will also be predominantly x-polarized. The x-component of the electric field lies primarily under the aperture, spreading with distance, and the z-component lies close to the aperture but under the metal, also spreading with distance. The field is most enhanced near the sharp edge of the aperture. There is a small component in the y-direction, as there must be for any small source of electric field. Its

magnitude is much smaller than the other's. The small size of the source precludes complete polarization, and the ratio of the two polarizations depends upon the numerical aperture of the collection lens[35]. Note that the scales for 1 nm separation are nearly ten times those at 10 nm. Also shown in the figure is the profile of the z-electric field times its gradient, which will be of interest later. The final plot represents integrals over images such as the others in the figure. It shows that all components of the electric field are enhanced, although the y-component remains quite small. In far field experiments using this geometry and weak lenses, there would be no y or z polarized light. The z-polarized component is relatively small even for high NA far-field objectives.

The apertureless probe must satisfy the same boundary conditions (only normal electric field) as any other conductor. This implies that the region of highest resolution, immediately under the tip will be predominantly of z-polarized electric field. This is indeed the case and has been shown in model calculations [17, 18]. This results in a difference in the nano-Raman spectra expected for samples with a fixed orientation under the probe, such as crystals and ordered adsorbates. The apetureless probe will see those modes excited by light in the z-direction, whereas the apertured probe will see all vibration modes. In the both cases, the tip can be withdrawn to alter the strength of the z-polarized interaction.

Near-field vs. Far-field Raman

Near-field Raman spectroscopy differs from conventional Raman spectroscopy in a variety of ways. These differences include a reduced Rayleigh tail, the presence of all polarization components of light [7], surface enhancement [5], light propagation considerations[36], surface plasmons, and gradient field effects[4]. The fact that there is a probe near the sample surface and the nature of the electric field at the probe make the near-field Raman experiments different from far field Raman experiments. With an understanding of the basic nature of the electric fields at the probe we now discuss consequences of those differences for near-field Raman spectroscopy.

Surface enhancement

From the Bethe Bouwkamp calculations, we understand the nature of the optical signal in the near-field for the apertured probe. As seen in figure 2, the electric field in all dimensions is largest at the aperture and decays exponentially with distance from the aperture. It is clear that the Raman signal from the sample surface should be enhanced. In the case of apertureless probes, Novotny has shown that enhancements in the signal at the metal probe apex can be obtained if the excitation light has a longitudinal component [17, 37]. The enhancement can be a factor of 1000 and it falls off exponentially with distance from the tip. The surface enhancement effect can be seen very clearly in work by Michaels with apertured probes and Anderson (among others) with apertureless. In Anderson's studies, there is no Raman signal until the probe is in the near-field of the sample [25]. Michaels shows the change in the Raman signal as a function of probe sample distance to be exponential in both transmission and reflection [24].

Propagation considerations

We have shown that some of the Raman active modes of KTP are enhanced as the probe approaches the surface. What is at first unexpected is that some modes are not enhanced in the measurement, especially when one considers Fig. 2, in which all components of the electric field are increased. Fig. 3 shows that this is indeed the case for nano-Raman of KTP measured in reflection with an apertured probe. The darker line in the figure shows a Raman spectrum taken about 35 nm from the surface of the KTP. The lighter line shows the difference of this spectrum with a far-field (but through the aperture) spectrum, taken with the tip several hundred nanometers back. We note that the dominant line of the spectrum, the A1 767 cm^{-1} mode of Yang et al. (1986), is absent in the difference. Another line, near 787 cm^{-1}, corresponding to the B1 peak of KTP, Ayars & Hallen (2000), that has been observed at 783 cm^{-1}, Yang et al. (1986), dominates the difference Raman spectrum. The B1 line is not Raman-allowed in the geometry of our far-field (tip retracted) experiment since it requires light polarized in the z-direction to excite it, and such electric field (figure 2) is only available when the probe is close to the surface. The A1 mode is in the plane of the surface so can be excited by far-field light. This observation is the key to understanding the absence of this mode in reflection NSOM Raman. Light must propagate from the oscillating dipole (at the Raman-shifted frequency) to the detector. To do this, it must move laterally under the tip, then scatter or diffract back towards the collection optics and, eventually, the spectrometer and CCD. However, the in-plane mode can only emit light with the electric field polarized parallel to the surface plane if it is to propagate laterally. This electric field is not allowed under the metal of the aperture, as schematically shown in figure 4, so the light reflects in a different direction. The light emitted by these modes in the near field is not observed in reflection. The farther field emission is the same in all the Raman spectra taken at different distances, so cancels.

Looking back at this discussion, two properties of the probe and sample are required for a peak to be not observable in the near field: it must lie in the plane of the surface, and the probe must extend sufficiently far to provide a propagation constraint. Note that this is not the same physics as quenching of emission when close to a metal surface[38]; we will discuss that later. This behavior simply results from dipole emission patterns and simple boundary conditions. This behavior is only expected for crystals and ordered layers of molecules on a surface. In this sense, it would be a good detector of order, for example, in self-assembled monolayers. Figure 4 illustrates that molecules with other orientations, even if excited by electric field in the plane of the surface, can still emit light in the near field that can propagate into the detection optics in reflection.

We note that if the same experiment was performed with collection in transmission rather than reflection, all modes should be observed and enhanced. This has both advantages and disadvantages. The advantage is observation of the modes. The disadvantage is that the B1 mode we see in Fig. 3 is very small compared to the far-field allowed A1 mode. With the spectral resolution used, the B1 mode would not be clearly identifiable. Since this mode's observation is of interest due to its distance dependence that follows a gradient-field rather than the field squared[4], it is useful to be able to

study it without interference from the nearby, stronger, A1 line. Propagation constraints can have benefits.

Apertureless NSOM does not have such a strong propagation constraint since the tip is so small. However, since only light with z-polarization is strongly enhanced, a requirement to identify it from the large background signal, vibrations excited only by electric field in the plane of the surface will not be observed with collection at any angle. Again, this result only applies to oriented samples.

Z polarization effects

For the case of the apertured probe, the presence of all polarization components allows for the possibility of the excitation of all Raman active modes. However, even though all modes may be excited, they may not reach the detector, so one must consider the propagation of light and the geometry of the sample. With those considerations in mind, it is possible to observe Raman modes that would normally be forbidden in a given experiment geometry. Indeed we have observed several Raman modes normally attributed to z-polarization in our near-field Raman work using optical fiber probes [7]. Figure 5 shows two Raman spectra on potassium titanyl phosphate ($KTiOPO_4$ or KTP), with light incident in the z-direction. These spectra are a micro-Raman spectrum and a near-field Raman spectrum that have been normalized to the strongest Raman line at 767 cm^{-1} (not shown) for comparison. The sample is excited by light polarized in the x-y direction for the micro Raman case. The fiber aperture lies in the x-y plane for the near-field spectrum. The micro-Raman spectrum shows a peak at 215 cm^{-1} which is an allowed peak for the experiment geometry. The near-field spectrum, however, shows a peak in this region that is shifted to higher wavenumber and broadened. This spectral change can be explained by the detection of the normally forbidden vibration mode at 220 cm^{-1}, which can only be excited by z-polarized light. Additionally, the peak at 268 cm^{-1} and the peak at 290 cm^{-1} are enhanced relative to other peaks. These peaks can be excited weakly or moderately with x-y geometry as can be seen in the micro-Raman spectrum, but these vibrations can be excited very strongly with a z-polarization. Finally, the micro-Raman spectrum has an allowed peak at 373 cm^{-1}. Again in the near field this peak is shifted and broadened, which can be explained by the peaks allowed in a z-polarization geometry at 368 cm^{-1}, 372 cm^{-1}, and 381 cm^{-1}.

Resolution and the Rayleigh Tail

Spatial resolution can affect the nano-Raman spectra, actually its background, even if the sample is homogeneous. Since the Raman process is very weak, the elastically scattered or nearly elastic (acoustic phonon scattered) light is many orders of magnitude larger than the Raman-shifted signal. If some of this light scatters from pointlike inhomogeneities (Rayleigh scattering) in the sampling region, it can enter the spectrometer in such a way as to appear as background for small wavenumbers. This is known as the Rayleigh tail, and is seen for the far-field measurement in Fig. 5 on the low wavenumber side of the graph. The near-field Raman data in the figure shows a dramatically reduced Rayleigh tail. We presume that this is due to the smaller sampled volume. It simply has fewer inhomogeneities that can act as scattering centers.

Gradient field effects

One of the most interesting spectroscopic effects that occurs in the near-field is a result of the presence of an electric field gradient, as is clearly seen in the Bethe-Bouwkamp calculations of Fig. 2. In the derivation of the Raman effect, the electric field is assumed to be constant. This is a very good assumption away from a metal surface, since the electric field there can only vary on the scale of the wavelength, which is at least three orders of magnitude longer than the typical excursion of an ion during a vibration. In the presence of a conductor, as in SERS and nano-Raman, the electric field can vary on the nanometer length scale, so the variation across a vibrating bond is not negligible. Qualitatively, this results in a variation of the Coulomb force over the course of the vibration, so provides a coupling to the vibration that is different from the standard Raman coupling. We call this gradient-field-Raman (GFR). A detailed derivation of this effect with more complete evidence is presented elsewhere [4, 39]. In brief, the selection rules for the GFR effect are very different from the usual Raman selection rules. The vibration must be optically active, but it can be either Raman active or IR active. The amplitude of the signal should be similar to that of the allowed Raman modes, and the relative strengths of the modes should be similar to those in infrared spectroscopy, for IR allowed modes. Additionally the GFR effect offers an alternative explanation for some of the spurious peaks observed in SERS where there is a strong electric field gradient due to the small metal colloids. The electric field gradient can also couple to vibrations via the quadrupole moment of the bond[40]. This is a physically different coupling mechanism. We will limit the discussion to GFR, although in most cases, both mechanisms will contribute to the signal, with relative weight depending upon the wavefunctions involved.

In order to study the GFR effect, we measured spectra on a KTP sample varying the distance between a fiber probe and the sample surface. The difference between the spectra far from the surface and the subsequent nearer spectra was plotted, and it revealed a peak that was shifted in energy from the original peak. The new peak is attributed to an IR vibration mode, which would be consistent with the GFR effect. When the area under this peak is plotted as a function of distance from the surface and modeled with both the GFR effect and an exponentially decaying electric field predicted by Bethe-Bouwkamp, we find that the GFR model gives a better fit to the data [5].

Surface Plasmons

Surface plasmons were discussed above, and are believed to be important for enhancing the field near an apertureless tip. They also can affect the emission of nano-Raman shifted light as a function of probe-sample separation. The final step of the Raman process is the emission of Raman-shifted light from an oscillating bond. Energy from the oscillating dipole that is emitting the Raman scattered light can be coupled into surface plasmons in a nearby conductor. There is a strong distance dependence to this coupling. The physics is similar to the changes in fluorescent lifetime with distance from a metal NSOM tip[38, 41, 42]. The physics is that the conditions for creation of surface plasmons rather than emission of light change rapidly as the metal-excited dipole distance varies. The effect can be to amplify the emission with enhanced reflection due to the

additional imaginary dielectric constant near the absorption, or to quench the emission as the energy is drained into creation of surface plasmons. The excited dipole is either the one that will fluoresce or the one that will emit the Raman-shifted light. Notice that the same principles are involved in both measurements. Raman scattering is preferred to study this effect since it is easier to sort out the polarization effects. These effects can be modeled [43]using the framework that has been developed for emission near metal surfaces[44-47]. As some of the references mention, it is important that the dipole be modeled as one with constant power emitted into all modes (light, plasmons, etc.) rather than a constant amplitude dipole. This is especially important when comparing different metal-emitter distances as we will see, since the coupling to non-radiative modes changes. Further, we have found in our own modeling that the polarization and angle of emission towards the surface can give strong effects.

Apertured vs. Apertureless

As we have seen, nano-Raman microscopy and spectroscopy can be accomplished with either apertured or apertureless probes. However, the two techniques are not equivalent. The electric fields under the aperture in fiber probes are very different from the electric fields under a metal tip. Under an aperture, all polarization components of the electric field are enhanced. Under an apertureless probe, only the z-component of the electric field is enhanced. In apertured nano-Raman, the x-y modes can be studied in transmission, and the z-modes can be studied in reflection or transmission. In apertureless only the z-polarization Raman modes are surface enhanced and can be studied. In the case of molecules that are randomly distributed, one can still measure all Raman active modes, as was pointed out in Fig. 4. One should be aware of the limitations of each technique when studying an ordered material.

Another consideration for apertureless NSOM is that the background Raman scattering signal must be subtracted to determine what is happening at the surface since Raman signal will be generated for light both near and far from the probe and along the entire path of the light towards the detection system. This can also be an issue in apertured systems, in which Raman from the silica forming the tip can give a measurable background if the aperture size is too large[48]. These effects are less important when imaging, as long as the signal from the surface exceeds the (counting) noise from the background, since contrast will be due to changes in the surface spectra.

While the fundamental limit on resolution does not differ significantly between apertured (10nm, since spatially resolved Raman resolution should equal fluorescence resolution)[13] and apertureless (also $\gtrsim$10nm) probes, larger signal levels have been obtained with the apertureless technique [30]. This means that higher resolution images can be obtained in reasonable times with the apertureless technique.

In summary, the two types of probes complement each other. If one wants to use propagation to block observation of modes in the near-field (while observing in the far field as reference lines), or to study x-y polarized modes on an oriented surface, then an apertured probe is called for. If, on the other hand the aim is to get the largest signal fastest measurement, or best practical resolution, an apertureless probe is a better choice.

Conclusion

In conclusion, there have been significant advancements in near-field Raman spectroscopy in particular in the area of improved probes resulting in improved signal, resolution, and imaging times. These include better apertured probes, apertureless probes, and coating probes with metal colloids to fabricate SERS probes. Near-field Raman offers the possibility of high resolution with surface sensitivity. However, when performing near-field Raman experiments, one should be aware that the nature of the near-field provides spectroscopic results that differ from what one would expect with conventional far-field Raman. One should be aware in particular of the polarized nature of light in the near-field exciting vibration modes that would otherwise be forbidden as well as extra peaks due to GFR effects and the requirement of propagation to the detector if the sample is highly oriented.

Acknowledgements

This work was supported by the National Science Foundation through grant DMR-9975543 and the Research Corporation through grant CC5342.

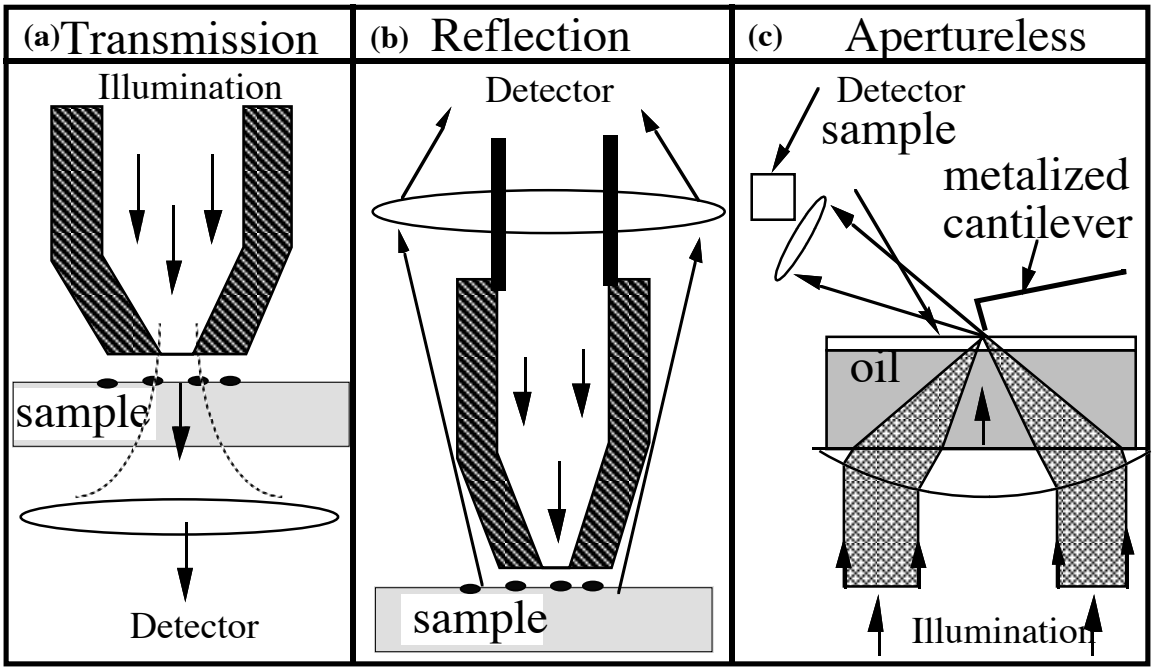

Figure 1 shows a cartoon of typical illumination mode apertured NSOM in transmission (a) and reflection (b) and apertureless NSOM in transmission (c).

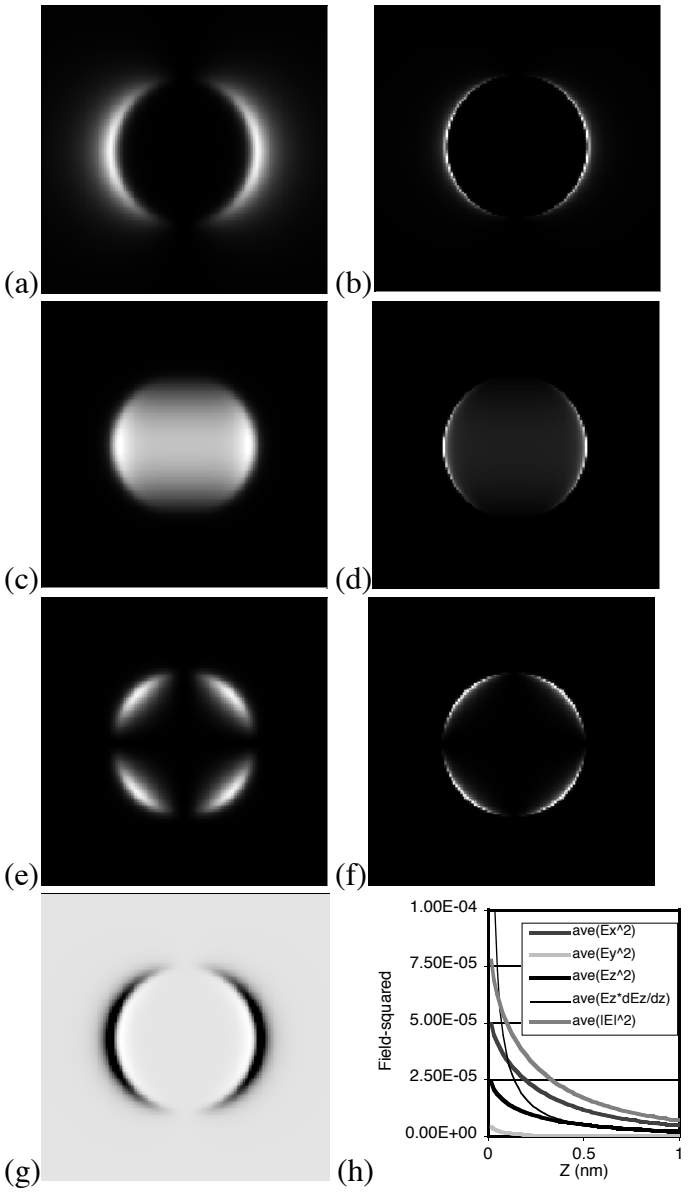

Figure 2. (a-f) Bethe-Boukamp model calculations of the electric field magnitude squared as a function of position in plane below the tip over a region 2 aperture sizes on a side with the tip centered. For the calculation, 514 nm light was used with a 200 nm aperture. The left column is calculated for a 10 nm tip-sample separation, and the right for a 1 nm separation. (a) and (b) show the z-component with gray range 0->0.7 and 0->7.0, respectively. (c) and (d) show the x-component with gray range 0->1.1 and 0->9.0, respectively. (e) and (f) show the y-component with gray range 0->0.14 and 0->1.4, respectively. (g) shows the electric field in the z-direction times its derivative with respect to z. It is nonzero both inside (where it is positive) and outside (where it is negative) the aperture. The integral over planes such as in (a-f) is shown in (h). The average electric field is shown for the different electric field components as a function of distance from the aperture in units of aperture size. In all cases, the electric field is enhanced near the aperture.

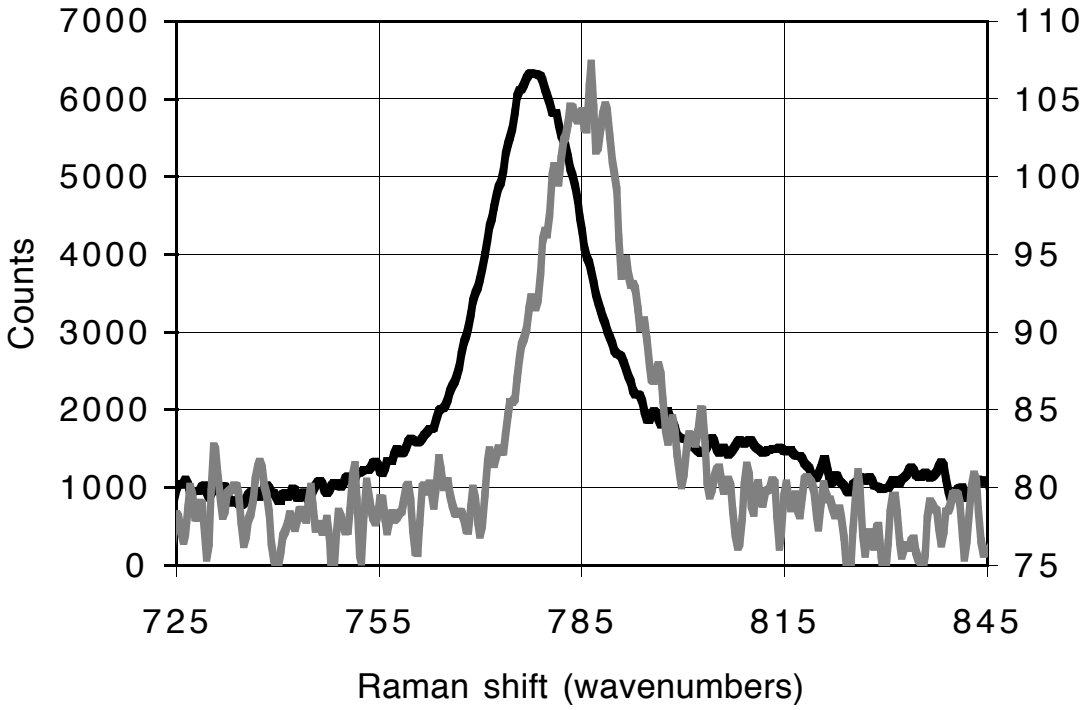

Figure 3. Raman spectra obtained with a metal coated fiber probe. The dark gray spectrum is obtained with the fiber tip about 35 nm from the sample surface. The light gray spectrum is the difference between the dark gray spectrum and a spectrum obtained far from the sample surface. The difference spectrum is shown with the scale on the right. Eighty counts have been added to the spectrum after subtraction.

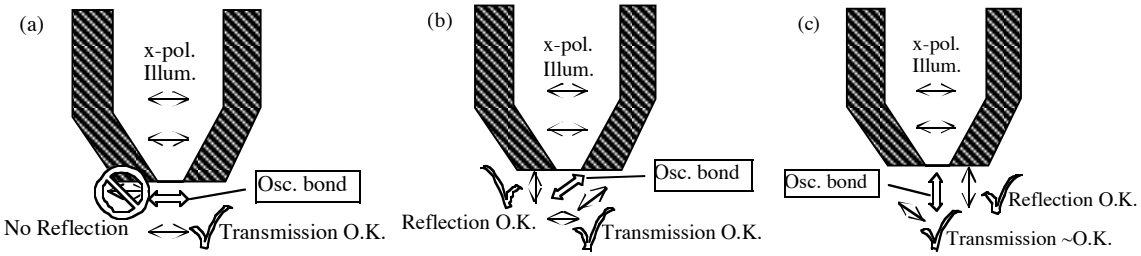

Figure 4. A schematic drawing that illustrates propagation constraints. (a) a dipole emitting Raman-shifted light in the plane of the surface is not detected in the reflection geometry, although it would be observable in transmission. (b) a tilted bond can be excited by x,y, or z-polarized light , and its emission is observed in reflection or transmission. (c) a bond in the z-direction needs z-polarized light for excitation, and its emission can be observed in reflection or transmission if a large enough collection angle is used.

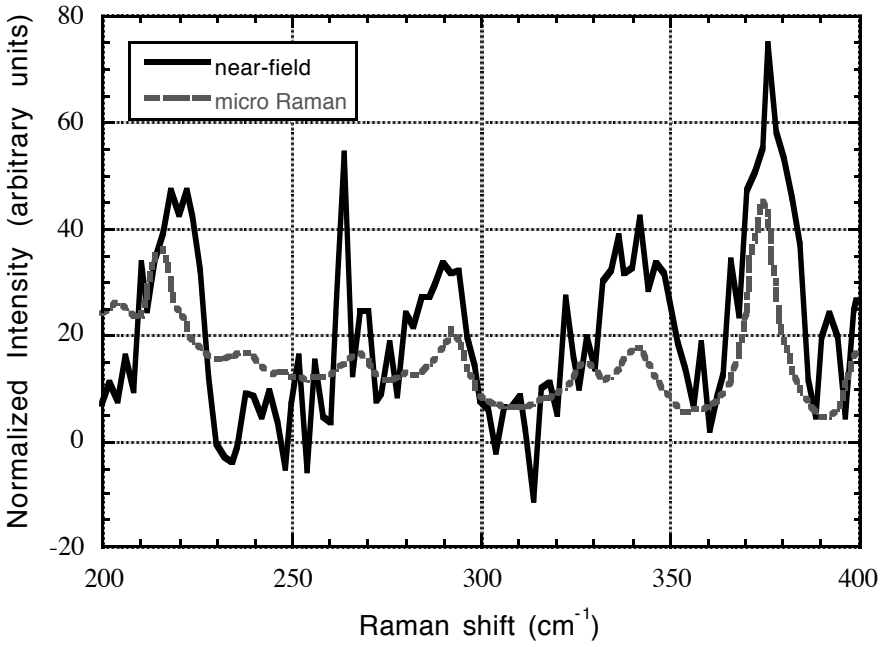

Figure 5 shows two normalized Raman spectra on KTP. The dashed line is a conventional micro-Raman spectrum, and the solid line is a near-field Raman spectrum. We note that the Rayleigh tail in the micro-Raman spectrum is not present in the near-field spectrum. The near-field peaks are enhanced relative to the micro-Raman peaks, and in many cases this can be attributed in part or in whole to the presence of a z-polarization component of the electric field at the aperture.

References

1. Jahncke, C.L., M.A. Paesler, and H.D. Hallen, Applied Physics Letters, 1995; **67**(17): 2483-2485.
2. Paesler, M.A., et al., Microscopy and Microanalysis, 1997; **3**: 815.
3. Zenhausern, F., M. P. O'Boyle, and H. K. Wickramasinghe, Appl. Phys. Lett., 1994; **65**: 1623.
4. Ayars, E.J., H.D. Hallen, and C. L. Jahncke, Physical Review Letters, 2000; **85**: 4180-4183.
5. Ayars, E.J., and H.D. Hallen, Applied Physics Letters, 2000; **76**(26): 3911-3913.
6. Hallen, H.D., E.J. Ayars, and C.L. Jahncke, Proceedings of the Seventh International Near-Field Optics Conference, 2002; **in press**.
7. Jahncke, C.L., H.D. Hallen, and M. A. Paesler., Journal of Raman Spectroscopy, 1996; **27**: 579-586.
8. Webster, S., D.A. Smith, D.N. Batchelder, S. Karlin, Synthetic Metals, 1999; **102**(1-3): 1425-1427.
9. Gucciardi, P.G., S. Trusso, C. Vassi, S. Patane, M. Allegrini, Physical Chemistry Chemical Physics, 2002; **4**(12): 2747-2753.
10. Zeisel, D., et al., Chemical Physics Letters, 1998; **283**(5-6): 381-385.
11. Goetz, M., D. Drews, D. R.T.Zahn, R. Wannemacher, Journal of Luminescence, 1998; **76-77**: 306-309.
12. Pohl, D.W., Denk W., and Lanz M., Applied Physics Letters, 1984; **44**(7): 651-653.
13. Betzig, E., et al., Science, 1991; **251**: 1468-1470.
14. Betzig, E., Isaacson M., and Lewis A., Applied Physics Letters, 1987; **51**(25): 2088-2090.
15. Betzig, E., et al., Applied Optics, 1992; **31**(No. 22): 4563-4568.
16. Inouye, Y., S. Kawata, Optics Letters, 1994; **19**: 159.
17. Novotny, L., Sanchez E.J., and Xie X.S., Ultramicroscopy, 1998; **71**: 21-29.
18. Furukawa, H., S. Kawata, Optics Communication, 1998; **148**: 221-224.
19. Valaskovic, G.A., Holton M., and G.H. Morrison, Appl. Opt., 1995; **34**(7): 1215.
20. Yakobson, B.I. and Paesler M.A., Ultramicroscopy, 1994; **57**: 204-207.
21. Sayah, A., C. Philipona, P. Lambelet, M. Pfeffer, F. Marquis-Weible, Ultramicroscopy, 1998; **71**: 59.
22. Suh, Y.D. and Zenobi R., Advance materials, 2000; **12**(15): 1139-1142.
23. Sqalli, O., M.P. Bernal, P. Hoffmann, and F. Marquis-Weible, Applied Physics Letters, 2000; **76**(15): 2134-2136.
24. Michaels, C.A., et al., Proceedings of SPIE the international society for optical engineering, 2000; **4098**: 152-159.
25. Anderson, M., Applied Physics Letters, 2000; **76**(21): 3130-3132.
26. Hayazawa, N., Y. Inouye, Z. Sekkat, S. Kawata, Optics Communication, 2000; **183**: 333-336.
27. Stöckle, R., Yung Doug Suh, Volker Deckert, Ranato Zenobi, Chemical Physics Letters, 2000; **318**: 131-136.
28. Zeisel, D., et al., Anal. Chem., 1997; **69**: 749.
29. Deckert, V., D. Zeisel, and R. Zenobi, Analytical Chemistry, 1998; **70**(13): 2646-2650.

30. Hayazawa, N., Y. Inouye, Z. Sekkat, S. Kawata, Journal of Chemical Physics, 2002; **117**(3): 1296-1301.
31. Christensen, D.A., Ultramicroscopy, 1994; **57**.
32. Novotny, L. in *Near-Field Optics*. 1995. San Diego: SPIE.
33. Bethe, H.A., Physical Review, 1944; **66**(Nos. 7 and 8): 163-182.
34. Bouwkamp, C.J., Phillips Research Report, 1950a; **5**: 401.
35. McDaniel, E.B., McClain S.C., and Hsu J.W.P., Applied-Optics, 1998; **37**(1): 84-92.
36. Hallen, H.D., Ayars E.J., and Jahncke C.L., Journal of Microscopy, 2002; **in press**.
37. Sanchez, E.J., Novotny L., and Xie X.S., Physical Review Letters, 1999; **82**(20): 4014-4017.
38. Bain, R.X., et al., Physical Review Letters, 1995; **75**: 4772.
39. Jahncke, C.L., E.J. Ayars, and H.D. Hallen., Proceedings Microscopy and Microanalysis, 2002: 1518CD.
40. Moskovits, M. and DiLella D.P., J. Chem. Phys, 1982; **77**(4): 1655-1660.
41. Ambrose, W.P., et al., Science, 1994; **265**: 364.
42. Xie, X.S. and Dunn R.C., Science, 1994; **265**: 361.
43. Hallen, H.D. and Ayars E.J.,; **in prep**.
44. Chance, R.R., Prock A., and Silbey R., *Molecular Fluorescence and Energy Transfer Near Interfaces*, in *Advances in Chemical Physics*, I.P.a.S.A. Rice, Editor, John Wiley and Sons: New York. p. 1.
45. Lukosz, W. and Kunz R.E., J. Opt. Soc. Amer, 1977; **67**: 1607.
46. Philpott, M.R., J. Chem. Phys., 1975; **69**: 499.
47. Weber, W.H. and Ford G.W., Physical Review Letters, 1980; **44**: 1774.
48. Jahncke, C.L. and Hallen H.D. in *9th annual meeting of IEEE Lasers and Electro-Optics Society (LEOS) 96*. 1996.